Title
Characterization of dentin and enamel by use of optical coherence tomography.

Journal
Applied optics, 38(10)

ISSN
1559-128X

Authors
Wang, XJ
Milner, TE
de Boer, JF
et al.

Publication Date
1999-04-01

DOI
10.1364/ao.38.002092

Characterization of dentin and enamel by use of optical coherence tomography

Xiao-Jun Wang, Thomas E. Milner, Johannes F. de Boer, Yi Zhang, David H. Pashley, and J. Stuart Nelson

Optical coherence tomographic images of human dentin and enamel are obtained by use of polarization-sensitive optical coherence tomography. A birefringence effect in enamel (λ = 856 nm) and light propagation along dentinal tubules are observed. The group index of refraction for both dentin and enamel was measured at 1.50 $\pm$ 0.02 and 1.62 $\pm$ 0.02, respectively. © 1999 Optical Society of America

OCIS codes: 170.1850, 170.4500, 260.1440, 290.3030.

1. Introduction

Optical coherence tomography is an effective imaging method for investigating the optical and structural properties of dental tissues. Understanding the origin of these properties will aid in the development of new optical methods for diagnosis of caries, measurement of tooth color, and therapeutic use of lasers. For example, detailed studies of light propagation in dental tissues are required for the development of laser dental treatment procedures.

Optical coherence tomography (OCT), an interferometric imaging technique to characterize the optical properties of various materials, is based on coherent cross-correlation detection of the interference fringe intensity of light backscattered from a test sample. This technique was initially introduced to identify and characterize closely spaced reflections in optical components used in the telecommunications industry.[1–3] Over the past few years, OCT has been applied by many investigators to image highly scattering biological tissues[4–7] with high spatial resolution ($<$15 μm). More recently, applications of polarization-sensitive OCT (PS-OCT) have also been reported.[8–10] In contrast to conventional OCT, in which the magnitude of backscattered light as a function of depth is imaged without accounting for polarization effects in the sample, PS-OCT measures the interference fringe intensity in two orthogonal polarization components of the backscattered light at each position in the sample and can be used to determine the magnitude of sample birefringence as a function of depth. Polarization-sensitive images of biological materials can reveal important structural information that is difficult to resolve with conventional OCT or other imaging techniques. In this paper we present optical low-coherence images of dentin and enamel in human teeth obtained with PS-OCT. Strong birefringence in enamel and anisotropic light propagation through dentinal tubules is observed. A group index of refraction for both dentin and enamel is determined from the OCT images.

Human teeth consist of three primary components: enamel, dentin, and pulp. As shown in Fig. 1, the bulk of the tooth consists of semitransparent dentin, which is thickest in the crown and gradually tapers as it reaches the apex of the root. Near the crown, the outer surface is covered by a thin and transparent layer of enamel that consists almost entirely of calcium salts in the form of large apatite crystals. The microcrystals form enamel prisms or rods with 4–6-μm transverse dimensions oriented normally to the tooth surface.[11] In the interprismatic space of enamel is protein, which occupies as much as 2% of the volume. Similar to bone, dentin consists of organic (30 vol. %), mostly collagen, fibrils and inorganic (50 vol. %) components incorporated into hydroxyapatite crystals and of water (20 vol. %). The main dentin structural component is

X.-J. Wang is with the Department of Physics, Georgia Southern University, Statesboro, Georgia 30460; e-mail address, xwang@gasou.edu. T. E. Milner is with the Biomedical Engineering Program, The University of Texas at Austin, Austin, Texas 78712. J. F. de Boer and J. S. Nelson are with the Beckman Laser Institute and Medical Clinic, University of California, Irvine, Irvine, California 92612. Y. Zhang and D. H. Pashley are with the Department of Oral Biology—Physiology, Medical College of Georgia, Augusta, Georgia 30912.

Received 29 April 1998; revised manuscript received 30 September 1998.

0003-6935/99/102092-05$15.00/0

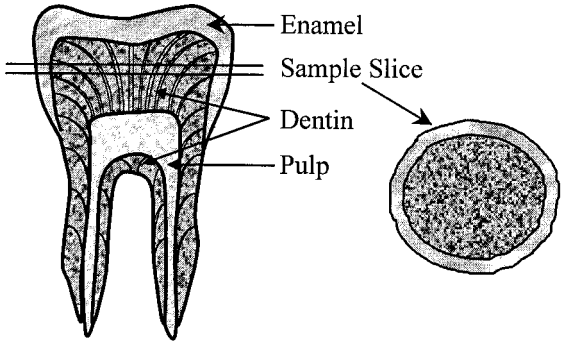

Fig. 1. Schematic of a sagittal section of a human molar (left) and a slab sample (right).

micrometer–sized dentinal tubules, which radiate with an S-shaped curve from the pulp cavity toward the periphery. In the innermost portion of the dentin, near the pulp, the tubule diameter is 3–4 μm, with number density of 7.5×10^4 mm^{-2}; in the outer portion, tubules narrow, with a lower number density of 3×10^4 mm^{-2}. As shown in Fig. 1, sample disks were prepared from the middle one-third of the crowns of extracted human third molars and sliced with an Isomet saw. The thickness of the sample disks varies from 300 μm to 1.0 mm.

2. Experiment

A schematic of the polarization-sensitive OCT instrumentation utilized in this study is shown in Fig. 2. Continuous near-infrared light (0.8 mW at $\lambda_0 = 856$ nm; FWHM $\Delta\lambda = 25$ nm) emitted by a superluminescent diode passes through a polarizer to give a pure vertical polarization state before division by a beam splitter into reference and probe beams. Light in the probe arm passes through quarter-wave plate QWP1 with the fast axis oriented at 45° to the vertical to provide circularly polarized light incident upon the sample. Light backscattered from the sample, after a return pass through QWP1, is in an arbitrary elliptical polarization state, determined by the birefringence and scattering properties of the sample. Light in the reference arm, after double passage through QWP2 with the fast axis oriented at 22.5° to the vertical, is linearly polarized at 45° to provide equal amplitudes with identical phase in vertical and horizontal polarization states. Light at the output of the interferometer is split by a polarizing beam splitter into horizontal and vertical polarization beams for detection by photoreceivers PR1 (horizontal) and PR2 (vertical), respectively. Optical power in the reference arm of the interferometer is attenuated by a neutral-density filter to reduce inherent intensity noise and thus improve the signal-to-noise ratio.[12] The optical phase of the superluminescent diode light in the reference arm of the interferometer is modulated (5.6 kHz) by a piezoelectric transducer attached to the reflection mirror.

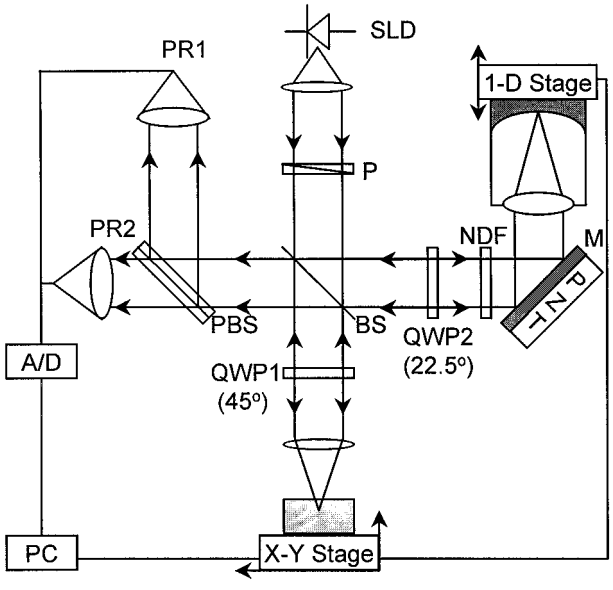

Fig. 2. PS-OCT instrumentation: SLD, superluminescent diode; P, polarizer; BS, beam splitter; PBS, polarizing beam splitter; NDF, neutral-density filter; M, reflection mirror; PZT, piezoelectric transducer; A/D, analog-to-digital converter; PC, personal computer; other abbreviations defined in text.

To reduce noise owing to Doppler shift fluctuations caused by variation in the axial translation velocity the sample is mounted upon a high-precision motorized X–Y stage and scanned parallel (lateral direction) to the sample surface. A small axial increment (~10 μm) is made perpendicular to the disk sample after each lateral scan, permitting the construction of a two-dimensional image. A single-axis translational stage driving the piezoelectric transducer is utilized to track the beam focus for each new axial position and maintain a zero optical path-length difference between the focus in the sample and the reference mirror such that interference fringe intensity is maximized.[13]

3. Results and Discussions

Figures 3(a)–3(d) show PS-OCT images of enamel extending from the air–enamel surface to the enamel–dentin junction; i.e., the lateral scan direction is along the enamel prisms. For each image, the light beam is incident perpendicular to the sample disk surface. Figures 3(a), 3(b), and 3(c) correspond, respectively, to images formed by detection of the horizontal polarization $[I_H(z)]$ component of light (PR1) as a function of depth z, by detection of the vertical polarization $[I_V(z)]$ component (PR2), and by the combination of PR1 and PR2 $[I_H(z) + I_V(z)]$, which in some cases is similar to a conventional OCT image. Figure 3(d) is a false-color birefringent image constructed by computing of $\mathrm{sgn}[I_H(z) - I_V(z)]10\log|I_H(z) - I_V(z)|$,[9] where $\mathrm{sgn}[I_H(z) - I_V(z)]$ is 1 when the difference of $[I_H(z) - I_V(z)]$ is positive and is −1 when the difference is negative. The bottommost feature in each image is formed by light reflection from the glass substrate. A banded structure that is characteristic of birefringence[9] is observed in Fig. 3(d) and can be attributed to enamel crystal prisms in the form of cut cylindrical fibers oriented

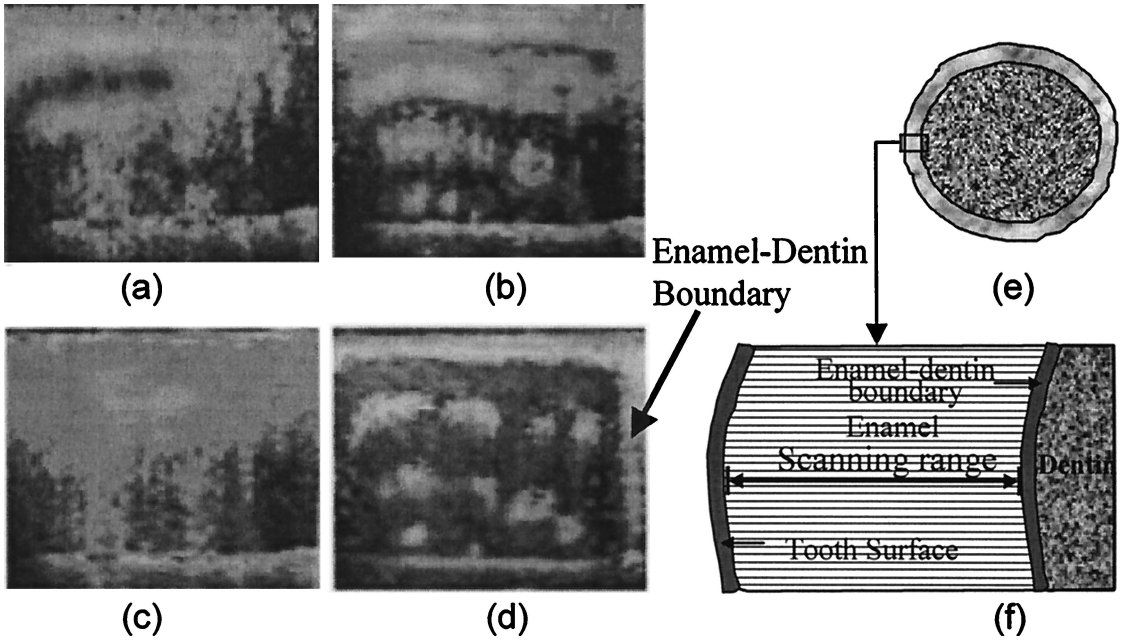

Fig. 3. (a)–(d) PS-OCT images of an enamel disk sample, 1.2 mm wide by 350 μm deep: (a) horizontal [$I_H(z)$], (b) vertical [$I_V(z)$], (c) sum of (a) and (b) [$I_H(z) + I_V(z)$], (d) birefringent image [$\mathrm{sgn}[I_H(z) - I_V(z)]10\log|I_H(z) - I_V(z)|$]. The enamel–dentin boundary is indicated. (e) Schematic of a tooth cross section, (f) enlargement of the scanned region. The thin lines in the enamel region represent prism cylinders. The lateral scan direction is parallel to the prism cylinders.

normally to the tooth surface, resulting in phase retardation between polarization components parallel and perpendicular to the crystal axis. The second and third bright bands appear broken, a feature that we believe is due to enamel tufts, or longitudinal fault planes (~100 μm in length and ~10 μm in width) in the sample volume. The tufts project outward along the enamel prisms from the enamel–dentin junction and are less mineralized.[14] When a lateral scan was made across the enamel prisms (orthogonal to the former scan) between the tooth surface and the enamel–dentin junction, an image with a smoother banded structure was observed. Because the scan direction is orthogonal to the longitudinal tufts and fewer tufts are present in this region, the broken-band feature observed in Fig. 3(d) disappeared.

Although dentin contains a considerable amount of collagen fibrils known to be birefringent, no features characteristic of birefringence are observed in PS-OCT images of dentin. We understand this observation because the collagen fibrils in dentin form a structurally irregular network extending over a wide spatial area[15,16] and are unlike the crystal prisms in the enamel region, which are arranged in a more orderly fashion parallel and perpendicular to the enamel surface. The collagen fibrils are positioned circumferentially around the surface of the dentinal tubules, yielding no birefringent effect when light propagates along the tubules that are estimated to cover ~20% of the surface area by their cross sections for the sample under test (see the next paragraph for a discussion of light propagation through the tubules). Between the dental tubules, in general, the course of collagen fibrils is perpendicular to the dentinal tubules and lies roughly in a plane parallel to the sample surface. Because the fibrils are randomly curved and cross linked within the plane, we do not observe birefringent features in PS-OCT images of dentin.

Figure 4(a) shows a PS-OCT image [$I_H(z) + I_V(z)$] recorded over a grid of points lying upon a diameter of the thin disk. Figure 4(b) shows the cross section corresponding to the tomographic image in Fig. 4(a). Various investigators have shown that the scattering processes in enamel and dentin can be described by a linear combination of forward-directed and diffuse isotropic components.[11,17] Inasmuch as the forward component is the dominant light-scattering process in dentin,[17] the isotropic component yields only a weak detected signal. To obtain more information relating to light propagation in dental materials, we place a reflecting mirror underneath the sample disk. Lines (L) at the right and left sides of the image represent reflections from the air–mirror interface without an overlying sample. Regions near the lines are recorded from the enamel ring of the disk, where the diffuse component is observed. Reflections from the front (R_1) and rear (R_2) surfaces of the enamel are observed. The feature just below the rear surface of the enamel (R_3) is the displaced image of the mirror (L). The dark areas between R_2 and R_3 represent the air gap between the mirror and the rear surface of the sample. Because the vertical displacement of the bottommost feature (R_4) from R_3 is twice that between R_2 and R_3, we believe that R_4 is due to a multiple reflection between the mirror and the rear enamel surface. The central portion of the image corresponds to dentin. The topmost surface feature

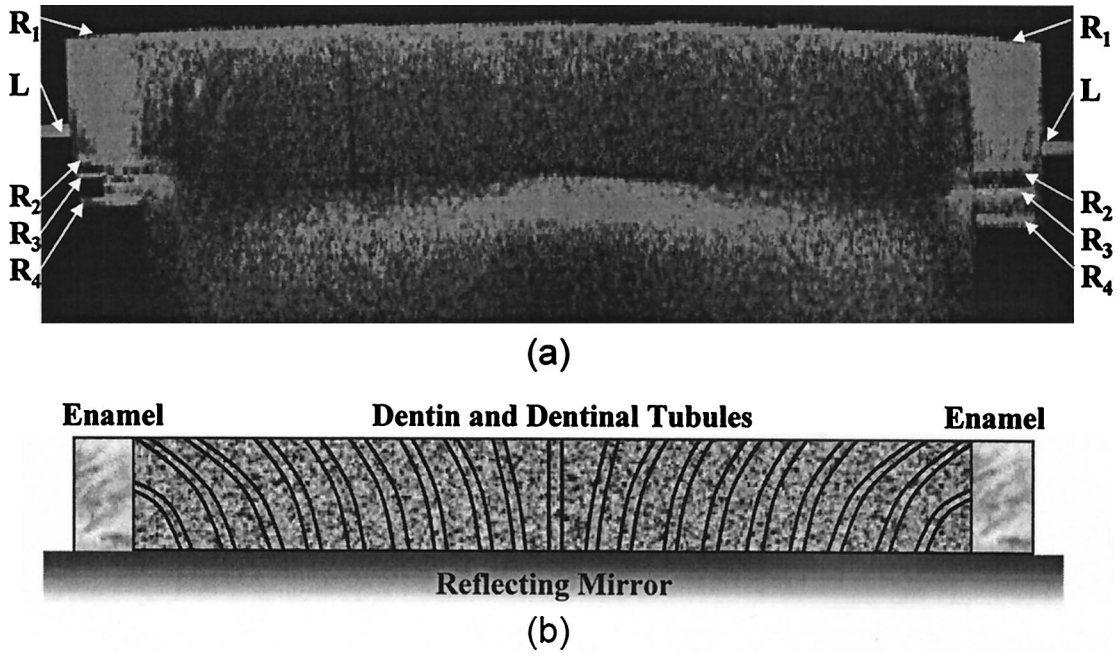

Fig. 4. (a) PS-OCT image [$I_H(z) + I_V(z)$] of a tooth sample extending through the diameter of the sample disk (10.8 mm wide by 600 μm deep). (b) Schematic of a tooth cross section corresponding to the PS-OCT image in (a).

is slightly curved as a result of the cutting procedure. The strongly curved feature in the lower central portion of the image represents light reflected from the mirror underlying the sample. Because the distribution of collagen fibrils among dentinal tubules is relatively uniform in our sample, the strongly curved feature may be due to anisotropic light propagation through the dentinal tubules.[11,18] As shown schematically in Fig. 4(b), the tubules near the disk center are oriented parallel to the propagation direction, and detected light that reflects from the mirror underlying the sample in this region has a relatively short optical path length. At radial positions farther from the center the tubules are oriented obliquely to the propagation direction, and detected light that reflects from the mirror underlying the sample in these regions has a relatively longer optical path length. At the dentin–enamel junction, tubules are oriented nearly perpendicularly to the propagation direction and produce strong attenuation of backscattered light with increasing depth.

Various investigators have provided experimental evidence and theoretical arguments for light guiding by dentinal tubules.[11,18] Knowledge of the local spatial variation in refractive index across the dentinal tubule is consistent with the existence of a light-guiding effect. Indeed, we have observed a light-guiding effect over distances longer than 2 mm in biological fibers.[7] Although the results of the present study do not prove the existence of light guiding by dentinal tubules, some conclusions can be drawn. The combined observation of the absence of macroscopic sample birefringence in dentin and of unequal optical path lengths of light propagating parallel and perpendicular to the tubules suggests that the strongly curved feature observed in Fig. 4(a) may be due to a scattering anisotropy. Such anisotropy has been noted by Fried *et al.*,[17] who observed in the far field a pronounced angular dispersion of light (λ = 1053 nm) scattered by dentinal tubules confined to a thin (80-μm) disk and oriented parallel to the propagation direction of the incident light. From the experiments of Fried *et al.* we can understand the nature of light propagation in thin dentin sections by noting that the measured far-field intensity is related to the field amplitude at the rear sample surface by a Fourier transform.[19] The observed pronounced angular dispersion of detected light indicates that the optical field at the rear surface of the dentin disk may be more spatially confined when tubules are oriented parallel to the direction of the incoming light. Therefore the scattering of light propagating in a direction perpendicular to the tubules in dentin may be stronger (μ_s is larger), more anisotropic (g is smaller), or both than for parallel directions. Because such a postulated variation of the anisotropy value (g) is consistent with light guiding by the tubules, we cannot distinguish which process is dominant in our experiments. We can conclude that the observed variation in light propagation through dentinal tubules may be a combined effect that is due to both scattering anisotropy and light guiding.

Figure 5 shows an enlarged portion of enamel taken from Fig. 4(a). Based on the measurement of ΔX_1, the optical path length of the sample, and ΔX_2, the apparent displacement of the mirror image, the group refractive index and the physical thickness of the sample can be determined simultaneously.[20,21] The average values of the group refractive indices of enamel and dentin at λ_0 = 856 nm are, respectively,

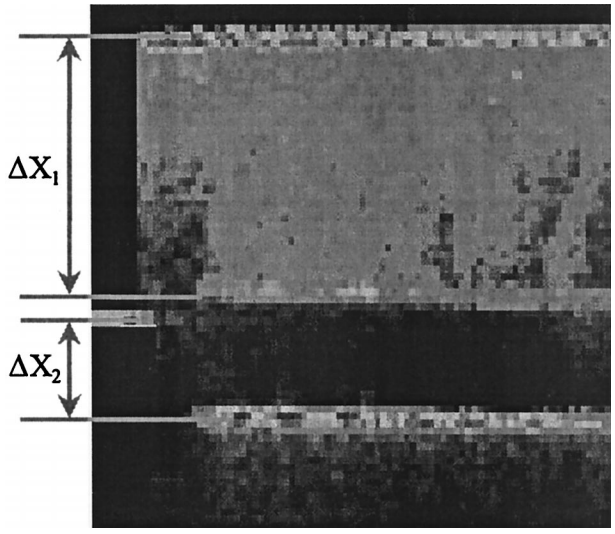

Fig. 5. PS-OCT image of enamel $[I_H(z) + I_V(z)]$ from which the group refractive index and the physical thickness of the sample (1.2 mm wide by 600 μm deep) are determined.

1.62 ± 0.02 (standard deviation) and 1.50 ± 0.02 (standard deviation). The values are consistent with previous measurements by other techniques in the visible spectral range.[22,23] To our knowledge, no refractive-index data for dentin and enamel in the infrared spectral region have been reported.

In conclusion, birefringence in enamel and an anisotropy effect of light propagation and scattering parallel and perpendicular to dentinal tubules have been observed by PS-OCT. Values of the group index of refraction have been measured for both dentin and enamel. The results may provide useful information for laser dental treatments. In the future PS-OCT may be applied for detection of dental caries in both enamel and dentin.

This study was supported by a National Institutes of Health training grant (to X.-J. Wang), by the Department of Physics, Georgia Southern University, and by grant DEO6427 from the National Institute of Dental & Craniofacial Research (to D. H. Pashley). The research of T. E. Milner is supported by the Whitaker Foundation and the National Institutes of Health. The contributions of J. S. Nelson and J. de Boer were supported by the National Institutes of Health, the U.S. Department of Energy, and the U.S. Office of Naval Research.

References

1. K. Takada, I. Yokohama, K. Chida, and J. Noda, "New measurement system for fault location in optical waveguide devices based on an interferometric technique," Appl. Opt. **26,** 1603–1606 (1987).
2. B. L. Danielson and C. D. Whitenberg, "Guide-wave reflectometry with micrometer resolution," Appl. Opt. **26,** 2836–2842 (1987).
3. R. C. Youngquist, S. Carr, and D. E. N. Davies, "Optical coherence-domain reflectometry: a new optical evaluation technique," Opt. Lett. **12,** 158–160 (1987).
4. D. Huang, E. A. Swanson, C. P. Lin, J. S. Schuman, W. G. Stinson, W. Chang, M. R. Hee, T. Flotte, K. Gregory, C. Puliafato, and J. G. Fujimoto, "Optical coherence tomography," Science **254,** 1178–1181 (1991).
5. J. M. Schmitt, A. Knüttel, and R. F. Bonner, "Measurement of optical properties of biological tissues by low-coherence reflectometry," Appl. Opt. **32,** 6032–6042 (1993).
6. J. A. Izatt, M. R. Hee, G. M. Owen, E. A. Swanson, and J. G. Fujimoto, "Optical coherence microscopy in scattering media," Opt. Lett. **19,** 590–592 (1994).
7. X. J. Wang, T. E. Milner, J. S. Nelson, R. P. Dhond, W. V. Sorin, and S. A. Newton, "Characterization of human scalp hairs by optical low-coherence reflectometry," Opt. Lett. **20,** 524–526 (1995).
8. M. R. Hee, D. Huang, E. A. Swanson, and J. G. Fujimoto, "Polarization-sensitive low-coherence reflectometer for birefringence characterization and ranging," J. Opt. Soc. Am. B **9,** 903–908 (1991).
9. J. F. de Boer, T. E. Milner, M. J. C. van Gemert, and J. S. Nelson, "Two-dimensional birefringence imaging in biological tissue by polarization-sensitive optical coherence tomography," Opt. Lett. **22,** 934–936 (1997).
10. M. J. Everett, K. Schoenenberger, B. W. Colston, Jr., and L. B. Da Silva, "Birefringence characterization of biological tissue by use of optical coherence tomography," Opt. Lett. **23,** 228–230 (1998).
11. G. B. Altshuler and V. N. Grisimov, "New optical effects in the human hard tooth tissue," in *Lasers and Medicine*, V. I. Konov, G. J. Mueller, and A. M. Prokhorov, eds., Proc. SPIE **1353,** 97–102 (1989).
12. W. V. Sorin and D. M. Baney, "A simple intensity noise reduction technique for optical low-coherence reflectometry," IEEE Photon. Technol. Lett. **4,** 1404–1406 (1992).
13. Z. Chen, T. E. Milner, D. Dave, and J. S. Nelson, "Optical Doppler tomographic imaging of fluid flow velocity in highly scattering media," Opt. Lett. **22,** 64–66 (1997).
14. A. Boyed, "Enamel," in *Teeth*, A. Oksche and L. Vollrath, eds. (Springer-Verlag, Berlin, 1989), pp. 309–473.
15. H. J. Höhling, "Special aspects of biomineralization of dental tissues," in *Teeth*, A. Oksche and L. Vollrath, eds. (Springer-Verlag, Berlin, 1989), pp. 475–524.
16. G. W. Marshall, Jr., S. J. Marshall, J. H. Kinney, and M. Balooch, "The dentin substrate: structure and properties related to bonding," J. Dent. **25,** 441–458 (1997).
17. D. Fried, R. E. Glena, J. D. B. Featherstone, and W. Seka, "Nature of light scattering in dental enamel and dentin at visible and near-infrared wavelengths," Appl. Opt. **34,** 1278–1285 (1995).
18. R. E. Walton, W. C. Outhwaite, and D. P. Pashley, "Magnification—An interesting optical property of dentin," J. Dent. Res. **55,** 639–642 (1976).
19. J. W. Goodman, *Introduction to Fourier Optics* (McGraw-Hill, New York, 1968), pp. 57–70.
20. W. V. Sorin and D. F. Gray, "Simultaneous thickness and group index measurement using optical low-coherence reflectometry," IEEE Photon. Technol. Lett. **4,** 105–107 (1992).
21. X. J. Wang, T. E. Milner, M. C. Chang, and J. S. Nelson, "Group refractive index measurement of dry and hydrated type I collagen films using optical low-coherence reflectometry," J. Biomed. Opt. **1,** 1–5 (1996).
22. D. Spitzer and J. J. ten Bosch, "The absorption and scattering of light in bovine and human dental enamel," Calcif. Tissue Res. **17,** 129–137 (1975).
23. J. R. Zijp and J. J. ten Bosch, "Theoretical model for the scattering of light by dentin and comparison with measurements," Appl. Opt. **32,** 411–415 (1993).